

Detecting Ships in the New Zealand Exclusive Economic Zone: Requirements for a Dedicated SmallSat SAR Mission

Jan Krecke ¹, Michelangelo Villano ², Senior Member, IEEE, Nertjana Ustalli ¹,
Andrew C. M. Austin ¹, Member, IEEE, John E. Cater, and Gerhard Krieger ², Fellow, IEEE

Abstract—The performance tradeoffs of a smallsat synthetic aperture radar (SAR) system for maritime surveillance in the coastal waters of New Zealand are investigated. The lower costs of smallsat platforms allow for a constellation of SAR satellites that can be launched from New Zealand using an existing local launch service provider. The minimum SAR image quality necessary for a smallsat system to achieve a desired detection performance is determined using existing X-band satellite data. The image quality is specified in terms of noise-equivalent sigma zero (NESZ) and resolution. It was found that for a resolution cell of 4 m^2 a system NESZ of -1.7 dB is sufficient to detect small fishing vessels with a probability of detection of 0.5, while maintaining the probability of false alarm below 10^{-10} . These requirements are translated into a preliminary SAR system design.

Index Terms—Synthetic aperture radar, radar remote sensing, low earth orbit satellites, satellite antennas, detectors, spaceborne radar, radar clutter, marine vehicles, sea surface.

I. INTRODUCTION

NEW Zealand is an emerging space-faring nation and is currently developing satellite technology and missions that provide tangible benefits to the country. These missions can take advantage of national capabilities, including a launch provider for small-satellites [1], ground stations [2], and a growing aerospace sector [3]–[5].

The location of New Zealand in the South Pacific ocean presents a significant challenge in reliably monitoring the exclusive economic zone (EEZ), which is approximately 4 million square kilometres [6]. The extent of the EEZ relative to the New Zealand mainland is shown in Fig. 1. There are strong economic and national security requirements to detect and monitor illegal, unreported and unregulated (IUU) fishing vessels in the EEZ.

Manuscript received December 19, 2020; revised February 9, 2021; accepted February 14, 2021. Date of publication March 2, 2021; date of current version March 26, 2021. The work of Jan Krecke was supported by a Graduate Scholarship from the Science for Technological Innovation (SfTI) programme, under Contract 2017 UOAX1706, funded by the New Zealand Ministry of Business, Innovation and Employment (MBIE). (Corresponding author: Jan Krecke.)

Jan Krecke and Andrew C. M. Austin are with the Electrical, Computer, and Software Engineering, The University of Auckland, Auckland 1010, New Zealand (e-mail: jkre504@aucklanduni.ac.nz; a.austin@auckland.ac.nz).

Michelangelo Villano, Nertjana Ustalli, and Gerhard Krieger are with the Microwaves and Radar Institute, German Aerospace Center, 82234 Wessling, Germany (e-mail: michelangelo.villano@dlr.de; Nertjana.Ustalli@dlr.de; gerhard.krieger@dlr.de).

John E. Cater is with the Engineering Science, The University of Auckland, Auckland 1010, New Zealand (e-mail: j.cater@auckland.ac.nz).

Digital Object Identifier 10.1109/JSTARS.2021.3062858

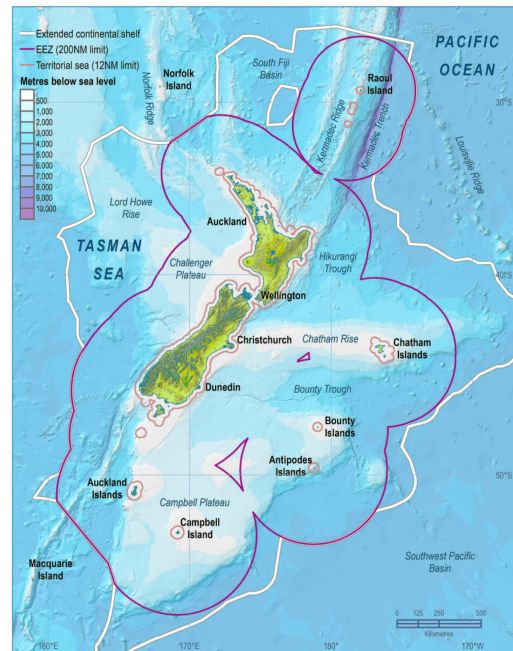


Fig. 1. Islands of New Zealand and surrounding ocean, including the EEZ outlined in red (adapted from [6]).

The ships of interest are typically 30 m in length and 7 m in width [7]. This size corresponds to a small overseas trawler. Ships smaller than these dimensions may occur in the EEZ, but will most likely not be an IUU vessel of interest. This is because most illegal fishing activities in New Zealand's EEZ are conducted by foreign ships with a port of call located several thousand kilometres away from New Zealand. Ships smaller than $30 \times 7 \text{ m}$ are unlikely to make such a journey.

Detection is currently achieved via patrol ships and sporadic flights by the New Zealand Defense Forces [8], however, this method only permits the identification of a small number of illegal ships, and the cost to identify a single ship is significant. This solution is not suitable for monitoring the entire EEZ, as the majority of illegal ships are not detected. Accordingly, spaceborne remote sensing, such as SAR, is under consideration.

SAR is an attractive solution, as it is capable of achieving regular coverage independent of weather conditions. Due to the small footprint size on the ground of typical SAR systems,

and the need for near real-time maritime surveillance, a group (or constellation) of small SAR satellites is required. Each satellite needs an SAR system optimized for detecting ships on the ocean surface. Preliminary design principles for small SAR systems have recently been proposed [9]. This work extends these ideas by proposing a cost-effective SAR mission with small satellites that benefits from a significant reduction of the power demands for a specific application scenario.

The aim of the ship detection SAR system described in this article is to improve on the current situation, in which almost all illegal ships are missed. Accordingly, constraints on the probability of detection P_d for a dedicated small-satellite SAR mission can be relaxed. In this article, a minimum P_d of 0.5 is deemed acceptable. Furthermore, a conservative ship detection algorithm is used as the general problem of ship detection is outside the scope of this article, as is the task of designing a ship detection system capable of high-fidelity detection in a wide variety of circumstances. For the probability of false alarm (PFA), the assumption is made that not more than two false alarms per whole coverage of New Zealand's EEZ are tolerable. This is to minimize the risk of unnecessarily deploying expensive resources, such as spotting aircraft or intercepting naval vessels. It is shown that this limit on the number of false alarms leads to a maximum permissible PFA of 1×10^{-10} .

In particular, this work identifies the minimum image requirements for an SAR system in order to detect typical fishing vessels with specified values for the PFA and probability of detection. Monte Carlo (MC) simulations are used to determine the probability of detection P_d for different image resolutions and different NESZ values. The PFA is determined numerically by assuming that pixels falsely exceeding a constant false alarm rate (CFAR) threshold are binomially distributed. Ambiguities are not considered explicitly, as ship targets are considered localized scatterers. Therefore, ambiguities can be easily removed in postprocessing, as they are defocussed and the locations are known [10]. In principle, the ambiguities could even be used to confirm the detection results by identifying patterns corresponding to the system's expected ambiguity locations.

SAR systems on larger satellites have been widely used for maritime surveillance; for example, both ERS-1 and Seasat [11]. Images from the Canadian Radarsat-1 have also been subject to various detection studies [12]–[14]. Similarly, its successor Radarsat-2 is used for ship monitoring as part of the Polar Epsilon project [15]. Another well-known SAR mission is TerraSAR-X [16]. While these satellites have been used for ship detection, this is not their primary mission objective. In particular, the small number of satellites limits the revisit time for maritime monitoring applications. However, recently, commercial missions are beginning to employ formations of multiple small-satellite platforms [17], [18]. The use of small, lightweight, and cost-effective platforms enables, in turn, the launch of more platforms for a given budget and paves the way for new mission design paradigms that are better suited to address emerging challenges such as the quasicontinuous monitoring of spatially limited areas.

The outline of this article is as follows. Section II illustrates how ship targets are modeled in the simulation process, and

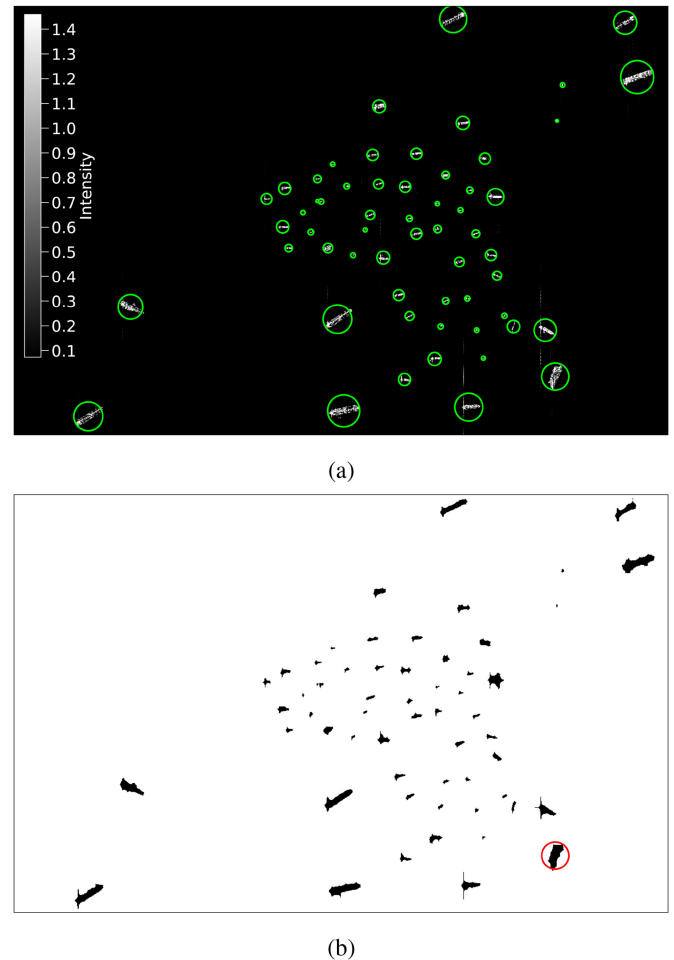


Fig. 2. TanDEM-X image used for statistical analysis of ship targets. (a) Original SAR image with target locations circled. (b) Processed pixel map, black pixels belong to a target, white pixels are clutter. The ECDF of the circled target is shown in Fig. 3.

describes the detection algorithm. Simplifying assumptions are also explained. Section III shows how simulations are used to derive requirements for the SAR image quality necessary to detect ships for a specified probability of detection and PFA. Section IV shows how these requirements can be translated into a simple system design. Finally, Section V presents the conclusions of this work.

II. METHODOLOGY

A. Statistical Properties of Ship Targets

A TanDEM-X [19] dataset has been analyzed with the goal of determining the appropriate intensity distribution of ship targets. In particular, the normalized target backscatter coefficient σ_{ship} is found, as this is necessary to determine the maximum NESZ sufficient for target detection.

Fig. 2(a) shows the TanDEM-X image used for the analysis.¹ The scene was acquired close to the port of Singapore, and was chosen due to the variety of apparent target sizes. The resolution

¹This dataset is taken from the EOWEB GeoPortal [20] and has HH-polarization.

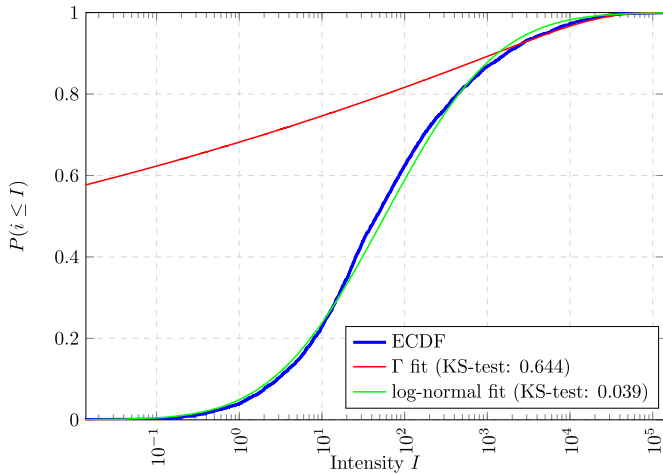


Fig. 3. ECDF for the target circled in Fig. 2(b), with fitted Γ and log-normal distributions.

of the image is 3×3 m, the extent of the scene is 6.5×10.1 km, and the image has been calibrated radiometrically. For visualisation, the intensities in Fig. 2(a) have been scaled, such that the range of values is between 1 to 20 times the mean of the original image. The image contains 58 targets of varying size. In order to determine the intensity statistics for each target, a decision has to be made for every pixel as to which target (or clutter) it belongs. This has been obtained by applying a multistage threshold algorithm to the original SAR image. The resulting pixel map is shown in Fig. 2(b).

In order to determine the distribution that best describes ships in the TanDEM-X data, two distributions are fitted to each target image: the Γ -distribution, according to the Swerling target models [21], and, as an alternative, the log-normal distribution.

A common goodness-of-fit test is the Kolmogorov–Smirnov (KS) test [22]. The KS-test compares the empirical cumulative density function (ECDF) obtained from the data with the fitted cumulative density function (CDF). Fig. 3 shows the ECDF and fitted CDFs for both the Γ -distribution and the log-normal distribution for the target circled in Fig. 2(b), and is typical of targets in this image. It is observed in Fig. 3 that the log-normal distribution describes the target data more accurately than the Γ -distribution, as is indicated by the KS-test: for the log-normal distribution the test statistic attains a value of approximately 0.04, whereas for the Γ -distribution it is 0.64. On average, the KS-statistic distribution for the entire dataset is 0.05 for the log-normal distribution, and 0.63 for the Γ -distribution.

The probability density function (PDF) of the log-normal distribution is [22]

$$f_{\ln}(I) = \frac{1}{I\beta\sqrt{2\pi}} e^{-\frac{(\log_e I - \alpha)^2}{2\beta^2}}. \quad (1)$$

The log-normal PDF is parameterized by the parameters α and β , which can be interpreted as the mean and standard deviation of the logarithm of the auxiliary data $y = \log_e I$, respectively, where I denotes the pixel intensity. Estimates for α and β for the 58 targets are shown in Fig. 4.

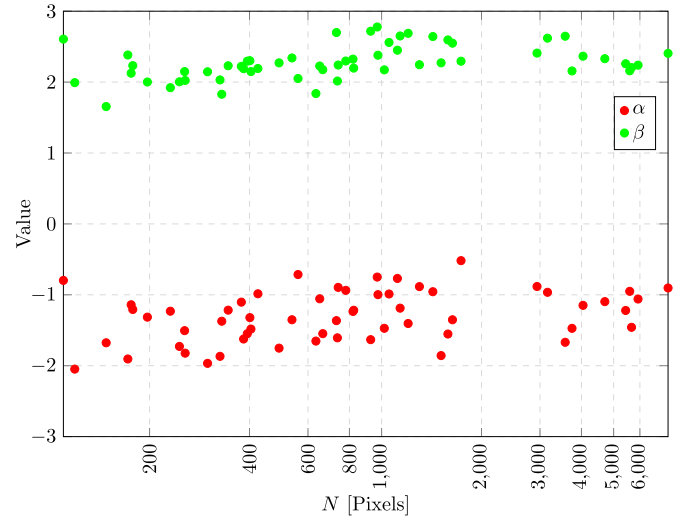


Fig. 4. Estimates for α and β for each target as a function of target size N in pixels.

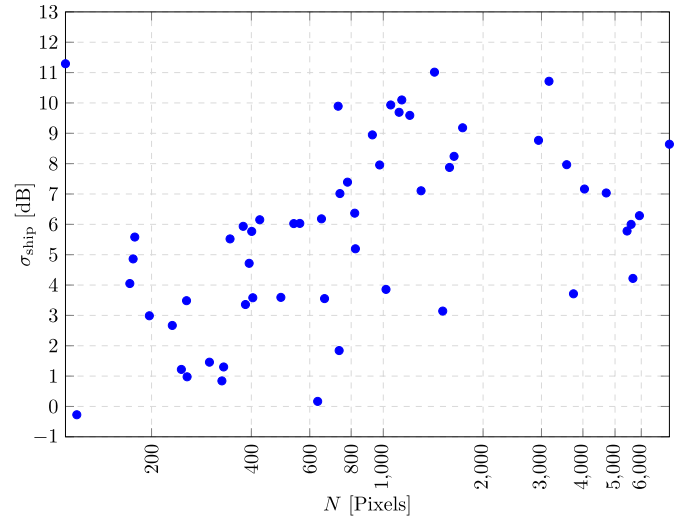


Fig. 5. Normalized target backscatter coefficient σ_{ship} versus target size N in pixels. Each data point corresponds to one target in Fig. 2.

In Fig. 4, it is observed that neither α nor β depend strongly on the target size N . Values for α and β can be used to compute σ_{ship} for each target

$$\sigma_{\text{ship}} = e^{\alpha + \beta^2/2}. \quad (2)$$

Fig. 5 shows the normalized backscatter coefficient σ_{ship} of the targets in Fig. 2 versus the target size in pixels. It is observed that smaller targets tend to be less reflective than larger ones. A target backscatter coefficient of $\sigma_{\text{ship}} = 2$ dB is assumed using the data in Fig. 5, as this is a conservative estimate for targets smaller than $N = 1000$ pixels. This value is based on the observation that in Fig. 5 more than 85% of the targets have a normalized backscatter coefficient larger than 2 dB.

B. Statistical Properties of Sea Clutter

It is important to know how the background pixels surrounding a target are distributed in order to apply a conventional

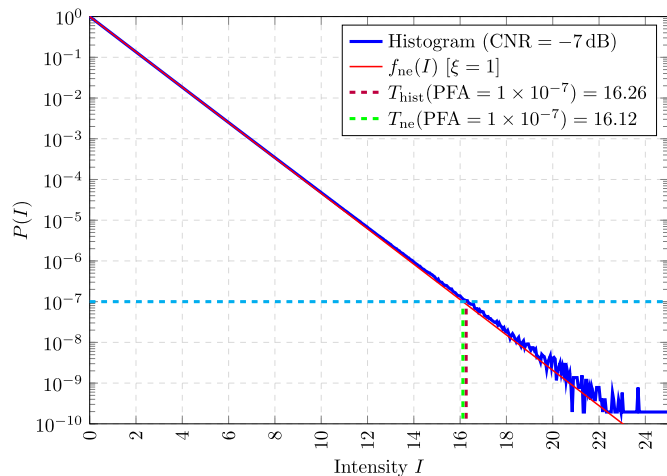


Fig. 6. MC simulation for $\text{CNR} = -7$ dB using 1×10^{11} simulated pixels. The normalized histogram of the pixel values obtained in the simulation is shown along with the PDF of the exponential distribution $f_{\text{ne}}(I)$ for $\xi = 1$. The clutter is modeled as a Γ -distributed RV with a texture parameter equal to 1.

CFAR ship detection algorithm [23]. Typically, radar returns from sea clutter are assumed to be K -distributed in the intensity domain [24]. However, this is computationally expensive to invert. In this article, a simpler approach based on experimental data is developed.

An analysis of TanDEM-X data reveals that the normalized backscatter coefficient of the sea surface is approximately -13 dB. Comparing this value to the target backscatter coefficient yields a signal-to-clutter ratio of 15 dB. Therefore, the power of the clutter returns is significantly below the thermal noise level, such that the clutter can be neglected, and that only thermal noise determines the distribution of the background pixels. This assumption may be violated for some acquisitions (e.g., in stormy conditions). The loss of acquisitions during such harsh conditions is, however, tolerable in view of the much less expensive system.

Using the radar equation and system parameters that could be realised by a small-satellite SAR system with low transmit power, it was found that the NESZ will be on the order of -3 dB (cf. Section IV), resulting in a clutter-to-noise ratio (CNR) of -10 dB. Assuming that the I - and Q -components of the noise follow a normal distribution, the intensity of the background pixels is negative exponentially distributed if the clutter is negligible [25].

The threshold T for a negative-exponentially distributed random variable (RV) can be computed by inverting its CDF, so that [22]

$$T = -\frac{1}{\xi} \log_e P_{\text{FA, goal}} \quad (3)$$

where $P_{\text{FA, goal}}$ is the desired PFA-value, ξ is the rate parameter of negative exponential distribution.

The decision to neglect clutter is supported by Fig. 6, which shows that the histogram of simulated SAR data with a CNR of -7 dB can be described by the PDF of the negative exponential distribution. The clutter is modeled as a Γ -distributed RV with

a texture parameter equal to 1. The low texture parameter indicates a high heterogeneity [25]. The low value for the texture parameter results in spiky sea clutter, which complicates ship detection due to the generally higher number of clutter pixels exceeding the detection threshold (or the noise floor, for the case presented), leading to more false alarms [24]. Therefore, the results presented are also valid for higher texture parameters or more homogeneous clutter.

Computing the CFAR threshold using (3) is computationally much less expensive than numerically inverting the K -distribution [26]. Therefore, neglecting the sea clutter significantly reduces the computational cost. It was found that the maximum CNR where this assumption remains valid is -7 dB. Similarly, a minimum NESZ of -6 dB is required when the normalised clutter backscatter is -13 dB.

C. Ship Detection in Simulated Data

The detection algorithm used for determining PFA and P_d differs from conventional ship detection algorithms in that a distinction is made between detection at the pixel level and detection at the object level.

The detection algorithm consists of two steps; first a CFAR algorithm is used to identify pixels bright enough to exceed a certain threshold [23]. This threshold is selected to yield a desired PFA when applied to background pixels that do not contain a target.

The detection algorithm used for the system requirement analysis is not the focus of this article, and accordingly is less complex than conventional approaches. The detection algorithm only serves to determine if detection with a small-satellite SAR system is feasible.

In order to group the pixels exceeding the threshold T , a simple counting algorithm is employed: a window with dimensions adjusted to the smallest expected target size is convolved with the CFAR pixel map. For each location of the target window, a minimum number n_{min} of pixels exceeding the threshold T have to be present for a target to be considered present.

In each iteration of the MC simulation, as many pixels as fit into a target detection box are simulated. The number N of simulated pixels depends on the target size of interest and the image resolution:

$$N = \left\lceil \frac{L_{\text{ship}} W_{\text{ship}}}{\delta_{\text{az}} \delta_{\text{rg}}} \right\rceil \quad (4)$$

where L_{ship} and W_{ship} are the length and width of the ship class of interest, and δ_{az} and δ_{rg} are the image resolution in azimuth and range, respectively.

The pixel intensity values must consist of exponentially distributed noise intensities and log-normally distributed target intensities. The generation of these samples can be expressed as

$$u = \left| \sqrt{t} e^{j\phi} + \underline{n} \right|^2 \quad (5)$$

where u represents the pixels used in the simulation, t stands for the log-normally distributed target pixels in the intensity domain, ϕ is the uniformly distributed phase of the target, and

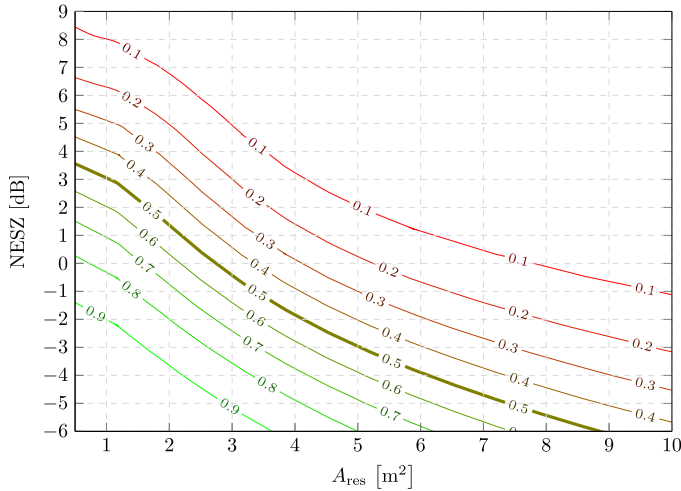


Fig. 7. Contours for probability of detection P_d as a function of the area of the resolution cell A_{res} and the NESZ. A system is considered to comply with design requirements if it achieves $P_d \geq 0.5$; this contour is shown in bold.

\underline{n} is complex Gaussian noise. In order to achieve an average noise intensity of 1, $\underline{n} \sim \mathcal{CN}(0, 1)$, where $\mathcal{CN}(a, b)$ indicates a complex Gaussian distribution with mean a and variance b .

In the case of no noise, $\underline{n} = 0$, then $u = t$, which follows the log-normal distribution by definition. If no target is present, $t = 0$, then $u = |\underline{n}|^2$, which can be shown to follow the exponential distribution [25].

For all simulations, target dimensions of $L_{\text{ship}} \times W_{\text{ship}} = 30 \times 7$ m and an azimuth resolution of $\delta_{\text{az}} = 2$ m are assumed. The range resolution δ_{rg} and the signal-to-noise ratio (SNR) are varied. To illustrate the simulated signal u , a range resolution of $\delta_{\text{rg}} = 2$ m and an SNR of 6 dB are assumed. Using (4), $N = 52$.

In the MC simulation, the signal u is generated M times; the probability of detection P_d is then approximated by dividing the number of targets exceeding the threshold n_{min} by the total number of targets M . Thus, P_d can be found for specific values of the CFAR-PFA ($P_{\text{FA, CFAR}}$) and the object threshold n_{min} . In order to specify these values, the desired PFA on object level $P_{\text{FA, obj}}$ has to be determined. Once $P_{\text{FA, obj}}$ is fixed, the survival function of the binomial distribution can be inverted to determine the value of $P_{\text{FA, CFAR}}$ necessary to obtain the desired $P_{\text{FA, obj}}$ for varying values of n_{min}

$$\begin{aligned}
 P(X \geq n_{\text{min}}) &= 1 - \sum_{i=0}^{n_{\text{min}}-1} \binom{N}{i} \\
 &\quad \times P_{\text{FA, CFAR}}^i (1 - P_{\text{FA, CFAR}})^{N-i} \\
 &= P_{\text{FA, obj}}. \tag{6}
 \end{aligned}$$

An analytical method of inverting (6) has not been found; therefore, a numerical approximation has been implemented.

III. IMAGE QUALITY REQUIREMENTS

The simulated dependence of the probability of detection P_d on the NESZ for different values of the resolution area A_{res} is shown in Fig. 7. The simulations were conducted for a desired PFA of $P_{\text{FA, goal}} = 1 \times 10^{-10}$. In the MC simulations,

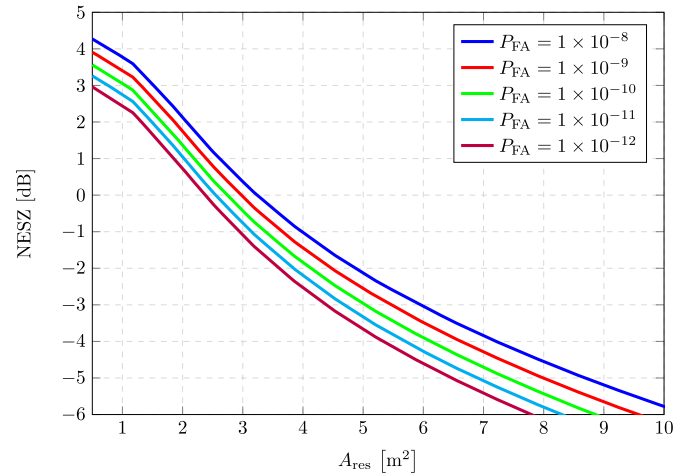


Fig. 8. Maximum NESZ necessary to achieve $P_d = 0.5$ versus resolution area A_{res} for varying $P_{\text{FA, goal}}$.

TABLE I
SYSTEM DESIGN PARAMETERS

Parameter	Symbol	Value	Units
Average transmit power	P_{avg}	15	W
Wavelength	λ	0.03	m
Antenna length	L_a	4	m
Antenna width	W_a	0.83	m
Antenna gain	G	46.66	dB
Look angle	γ	40	$^\circ$
Orbit height	H	500	km
Satellite velocity	v	7100	m s^{-1}
Noise temperature	T_s	300	K
Noise figure	F	5	dB
System losses	L	5	dB
Rx bandwidth	B_r	100 & 140	MHz

a resolution cell is either completely filled by a target or clutter. This leads to a discretization error for the P_d -values, which is reduced using a Gaussian filter. For each individual data point in Fig. 7, the combination of n_{min} and $P_{\text{FA, CFAR}}$ that yields the highest value for P_d while keeping $P_{\text{FA, obj}}$ at the desired value of $P_{\text{FA, goal}}$ has been selected. Fig. 7 shows that to achieve a probability of detection of at least 0.5, an NESZ of more than -5.5 dB is sufficient if the resolution cell is 10 m^2 or less.

Fig. 8 shows how the requirements for NESZ and A_{res} change if the constraints on $P_{\text{FA, goal}}$ are tightened or relaxed. The desired value for P_d has been set to 0.5 and with a decreasing $P_{\text{FA, goal}}$ the required NESZ also decreases as expected. However, the difference in required NESZ for different values of $P_{\text{FA, goal}}$ is only on the order of a few dB. This implies that changing the number of false alarms by one or two orders of magnitude does not significantly affect the system design in terms of resolution or NESZ.

IV. PRELIMINARY SYSTEM DESIGN

This section explores how the relationship between maximum NESZ and resolution cell area can be translated into an initial SAR-system design.

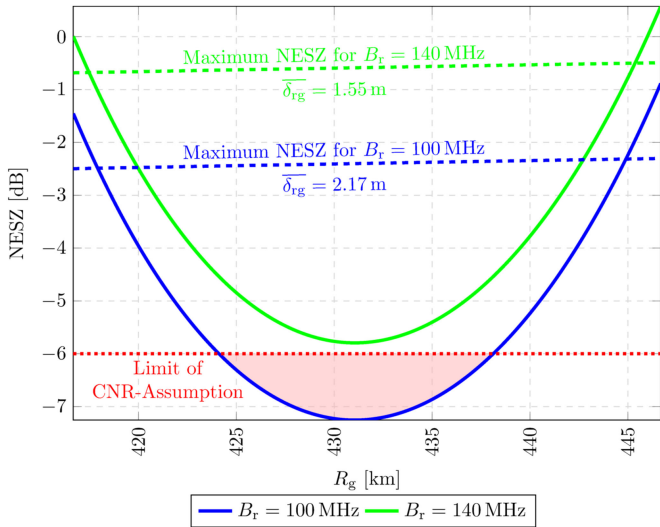


Fig. 9. NESZ versus ground range for system parameters shown in Table I and two different bandwidths ($B_r = 100$ MHz and 140 MHz); the corresponding mean range resolutions are $\delta_{rg} = 2.17$ m and 1.55 m). The required NESZ (dashed lines) for each bandwidth correspond to $P_d = 0.5$ and $P_{FA, goal} = 1 \times 10^{-10}$. The plot shows the NESZ within the 3 dB beamwidth of the antenna beam on the ground. The shaded area indicates NESZ values, which do not comply with the assumptions made for the simulations in Section III.

The NESZ is computed using the parameters in Table I by

$$\text{NESZ} = \frac{256\pi^3 r^3 B_r \sin \theta_i v k T_s \text{FL}}{P_{avg} G^2 \lambda^3 c} \quad (7)$$

where c is the speed of light, θ_i is the angle of incidence, and r is the range from the satellite to ground. The range r and the satellite altitude H are connected by the relationship $H = r \cos \theta$. All other parameters are shown in Table I [10].

The desired object PFA is set to $P_{FA, obj} = 1 \times 10^{-10}$. It can be shown that this value corresponds to approximately two false object detections per complete coverage of the area of interest ($A_{EEZ} \approx 4 \times 10^6 \text{ km}^2$): The number of target detection windows N_{win} present in the entire area of interest A_{EEZ} can be approximated by

$$N_{win} \approx \frac{A_{EEZ}}{L_{ship} W_{ship}} = 19.05 \times 10^9. \quad (8)$$

The required PFA to achieve $N_{FA} = 2$ per whole coverage is then $P_{FA, obj} = N_{FA}/N_{win} \approx 1 \times 10^{-10}$.

The parameters in Table I were chosen because they can reasonably be implemented on a small-satellite platform. In particular, the SAR transmit power is low compared to typical state-of-the-art SAR systems [19], due to the limited power available from small solar panels. The look-angle γ and the antenna width W_a have been optimized to give a 3 dB beamwidth on the ground of at least 30 km.

The NESZ computed with (7) is plotted over the ground range R_g in Fig. 9 for two different values of the bandwidth B_r , corresponding to two different range resolutions. It should be noted that the NESZ requirements shown as dashed lines in Fig. 9 are adjusted for the appropriate range resolution. It is observed that for both bandwidths the system NESZ is better than required over a ground range of almost 30 km. As expected from (7), the NESZ falls off with decreasing B_r . This means that

the system becomes more sensitive to radar returns from weak scatterers, while simultaneously causing the range resolution to become coarser. The dashed lines in Fig. 9 show that the required NESZ also decreases when the bandwidth is reduced. This is in agreement with Fig. 8, which shows that for a coarser resolution a more sensitive system is required to detect a target with the same probability P_d . For both bandwidths, Fig. 9 shows that the ground range over which the NESZ requirement is fulfilled is almost identical.

For $B_r = 100$ MHz, the resulting NESZ curve is partially below the -6 dB threshold derived in Section II. Therefore, the NESZ values below the threshold may differ from what would be obtained if the sea clutter was taken into account in the simulations.

V. CONCLUSION

This article focuses on the design of a small-satellite SAR system for dedicated maritime surveillance in the New Zealand EEZ. A methodology was developed to assess the impact of ship detection requirement on the design of an SAR system. A simplified situation and model were used to demonstrate the process. Results apply only to this case, however, the methodology can be applied to other cases.

Specifically, TanDEM-X data were analyzed in order to extract statistical models of ship targets. It was found that the log-normal distribution is an appropriate fit for these targets. It was also shown that for a CNR below -7 dB, the sea clutter contribution to the radar signal can be neglected. This was shown by simulating heterogeneous sea clutter with additive Gaussian noise. With the normalized target backscatter coefficient found from the data, the minimum NESZ for which the assumption is valid is -6 dB.

To detect ships with dimensions 30×7 m, a curve has been computed that relates the maximum permissible NESZ to the resolution for a desired probability of detection of 0.5 and PFA of 1×10^{-10} (which represents two false alarms over the entire EEZ). For example, with a resolution cell of 4 m^2 , the system NESZ must not exceed -1.7 dB, whereas at a resolution of 8 m^2 , the maximum NESZ is -5.4 dB.

Future work will focus on a more detailed system design. Various methods of improving the system performance will be considered. For example, given that short revisit times are crucial for maritime surveillance, a concept of operations for a constellation of small satellites will be explored.

REFERENCES

- [1] "Rocket Lab." Accessed: Feb. 1, 2021. [Online]. Available: <https://www.rocketlabusa.com>
- [2] "Awarua Satellite Ground Station." Accessed: Feb. 1, 2021. [Online]. Available: <https://awaruasgs.com>
- [3] "Te Punaha Atea—Auckland Space Institute." Accessed: Feb. 1, 2021. [Online]. Available: <https://space.auckland.ac.nz/>
- [4] "Christchurch Aerospace." Accessed: Feb. 1, 2021. [Online]. Available: <https://www.christchurch.space/>
- [5] "New Zealand SpaceAgency." Accessed: Nov. 18, 2020. [Online]. Available: <https://www.mbie.govt.nz/science-and-technology/space/>
- [6] New Zealand Ministry for the Environment, "New Zealand's marine environment," Accessed: Nov. 20, 2020. [Online]. Available: <https://www.mfe.govt.nz/publications/marine-environmental-reporting/our-marine-environment-2016-introduction-our-marine>

- [7] H. A. Karanassos, *Commercial Ship Surveying: On/Off-Hire Condition Surveys and Bunker Surveys*. Oxford, U.K.: Elsevier, 2016.
- [8] "Antarctic toothfish poaching ships shrug off New Zealand navy." Accessed: Nov. 11, 2020. [Online]. Available at <https://www.theguardian.com/environment/2015/jan/21/antarctic-toothfish-poaching-ships-shrug-off-new-zealand-navy>
- [9] A. Freeman, "Design principles for smallsat SARs," in *Proc. 32nd Annu. AIAA/USU Conf. Small Satell.*, 2018.
- [10] J. C. Curlander and R. N. McDonough, *Synthetic Aperture Radar: Systems and Signal Processing*. Hoboken, NJ, USA: Wiley, 1991.
- [11] K. Eldhuset, "An automatic ship and ship wake detection system for spaceborne SAR images in coastal regions," *IEEE Trans. Geosci. Remote Sens.*, vol. 34, no. 4, pp. 1010–1019, Jul. 1996.
- [12] P. W. Vachon, J. Campbell, C. Bjerkelund, F. Dobson, and M. Rey, "Ship detection by the RADARSAT SAR: Validation of detection model predictions," *Can. J. Remote Sens.*, vol. 23, no. 1, pp. 48–59, 1997.
- [13] P. W. Vachon, S. Thomas, J. Cranton, H. Edel, and M. Henschel, "Validation of ship detection by the RADARSAT synthetic aperture radar and the ocean monitoring workstation," *Can. J. Remote Sens.*, vol. 26, no. 3, pp. 200–212, 2000.
- [14] C. C. Wackerman, K. S. Friedman, W. G. Pichel, P. Clemente-Colón, and X. Li, "Automatic detection of ships in RADARSAT-1 SAR imagery," *Can. J. Remote Sens.*, vol. 27, no. 5, pp. 568–577, 2001.
- [15] P. W. Vachon, C. Kabatoff, and R. Quinn, "Operational ship detection in Canada using RADARSAT," in *Proc. IEEE Geosci. Remote Sens. Symp.*, 2014, pp. 998–1001.
- [16] S. Brusch, S. Lehner, T. Fritz, M. Soccorsi, A. Soloviev, and B. van Schie, "Ship surveillance with TerraSAR-X," *IEEE Trans. Geosci. Remote Sens.*, vol. 49, no. 3, pp. 1092–1103, Mar. 2011.
- [17] "ICEYE Homepage." Accessed: Nov. 10, 2020. [Online]. Available: <https://www.iceye.com/>
- [18] "Capella Space Homepage." Accessed: Nov. 10, 2020. [Online]. Available: <https://www.capellaspace.com/>
- [19] G. Krieger *et al.*, "TanDEM-X: A satellite formation for high-resolution SAR interferometry," *IEEE Trans. Geosci. Remote Sens.*, vol. 45, no. 11, pp. 3317–3341, Nov. 2007.
- [20] "Dataset used for ship target analysis." Accessed: Nov. 13, 2020. [Online]. Available: https://eoweb.dlr.de/guestegp/productDetails/TDM-CoSSC-Experimental:/dims_op_pl_dfd_XXXXB00000000447167885478/dims_op_pl_dfd_/TDM.SAR.COSSC.details
- [21] P. Swerling, "Probability of detection for fluctuating targets," *IRE Trans. Inf. Theory*, vol. 6, no. 2, pp. 269–308, 1960.
- [22] Y. Dodge, *The Concise Encyclopedia of Statistics*. New York, NY, USA: Springer, 2008.
- [23] D. Crisp, "The state-of-the-art in ship detection in synthetic aperture radar imagery," *Defence Sci. Technol. Org.*, Port Wakefield, SA, Australia, Res. Rep. DSTO-RR-0272, 2004.
- [24] K. D. Ward, S. Watts, and R. J. Tough, *Sea Clutter: Scattering, the K Distribution and Radar Performance*, 2nd ed. Stevenage, U.K.: IET, 2013.
- [25] C. Oliver and S. Quegan, *Understanding Synthetic Aperture Radar Images*. Raleigh, NC, USA: Scitech, 2004.
- [26] S. K. Joshi, S. V. Baumgartner, A. B. da Silva, and G. Krieger, "Range-doppler based CFAR ship detection with automatic training data selection," *Remote Sens.*, vol. 11, no. 11, p. 1270, 2019.



Jan Krecke received the B.Eng. in telecommunications engineering from the Baden-Württemberg Cooperative State University, Friedrichshafen, Germany in 2015. In 2018 he received the M.Sc. in Electrical Engineering from the Technical University of Munich, Munich, Germany.

From 2012 to 2015 he was working as dual student with Airbus Defence and Space in Munich, and Bangalore, India. From 2015 to 2018 he was a working student with Airbus Defence and Space in Munich, Germany. In September 2018 he joined the

University of Auckland to do his Ph.D in Electrical Engineering and Information Technology with the Department of Electrical, Computer, and Software Engineering. His research interests include image processing and radar systems.



Michelangelo Villano (Senior Member, IEEE) received the B.Sc. and M.Sc. degrees (Hons.) in telecommunication engineering from the Sapienza University of Rome, Rome, Italy, in 2006 and 2008, respectively, and the Ph.D. degree (Hons.) in electrical engineering and information technology from the Karlsruhe Institute of Technology, Karlsruhe, Germany, in 2016.

From 2008 to 2009, he was a Young Graduate Trainee with the European Space Research and Technology Center, European Space Agency, Noordwijk, The Netherlands, where he developed processing algorithms for ice sounding radar. In 2017, he was a Visiting Research Scientist with the Communications, Tracking, and Radar Division, NASA Jet Propulsion Laboratory, Pasadena, CA, USA, where he analyzed novel acquisition modes for the NASA Indian Space Research Organization synthetic aperture radar (SAR) instrument. Since 2009, he has been with the German Aerospace Center (DLR), Microwaves and Radar Institute, Wessling, Germany, where he is currently the Head of the NewSpace SAR Research Group. Since 2019, he has also been a Lecturer with Ulm University, Ulm, Germany. He has authored or coauthored more than 80 research articles in peer-reviewed journals and international conference proceedings. He holds eight patents in the field of SAR. His research interests include the conception of innovative SAR modes for high-resolution wide-swath imaging and the development of low-cost SAR solutions for frequent and enhanced Earth monitoring.

Dr. Villano has been a member of the Technical Program Committee of the European Conference on SAR (EUSAR), since 2016. He was a recipient of the First Place Student Paper Award at the EUSAR, Berlin, Germany, in 2014, the IEEE Geoscience and Remote Sensing Society Letters Prize Paper Award, in 2015 and 2017, the Student Paper Award at the Asia-Pacific Conference on Synthetic Aperture Radar, Marina Bay Sands, Singapore, in 2015, the DLR Science Award, in 2016, the Award as Young Scientist of the Foundation Werner von Siemens Ring, in 2017, the ITG Dissertation Award, in 2017, and the Best Paper Award at the German Microwave Conference 2019. He is Co-Chair of the Working Group on Remote Sensing Instrument and Technologies for Small Satellites of the IEEE Geoscience and Remote Sensing Society's Technical Committee on Instrumentation and Future Technologies. He is currently an Associate Editor for the IEEE GEOSCIENCE AND REMOTE SENSING LETTERS. He was a Guest Editor for the special issues Advances in Antenna Array Processing for Radar 2014 and Advances in Antenna Array Processing for Radar 2016 of the International Journal of Antennas and Propagation.



Nertjana Ustalli received the M.Sc. degree (*cum laude*) in communication engineering and the Ph.D. degree in radar and remote sensing from Sapienza University of Rome, Rome, Italy, in July 2014 and February 2018, respectively.

From July 2018 to June 2019, she was a Postdoctoral Researcher with the Department of Information Engineering Electronics and Telecommunications (DIET), Sapienza University of Rome, where she worked on the development of detection and motion parameters estimation techniques of moving targets from Forward Scatter Radar configuration. Since October 2019, she is with the Microwaves and Radar Institute, German Aerospace Center (DLR), Wessling, Germany. Her current research interest includes development of cost-effective synthetic aperture radar for dedicated application.

Dr. Ustalli was the recipient of the Best Student Paper Award at the 2017 International Conference on Radar Systems, Belfast, U.K., the Best Paper Award at the 2018 International Radar Symposium (IRS2018), Bonn, Germany, the Best Paper Award at the 2018 GTTI Workshop on Radar and Remote Sensing, Pavia, Italy, and the Best 2018 Ph.D. thesis defended at an Italian University in the areas of communications technologies at the GTTI annual reunion, Bari, Italy.



Andrew C. M. Austin (Member, IEEE) received the B.E. (Hons.) and Ph.D. degrees in electrical and electronic engineering from the University of Auckland, Auckland, New Zealand, in 2007 and 2012, respectively.

From 2011 to 2013, he was a Postdoctoral Fellow with the Electromagnetics Group, University of Toronto, Toronto, ON, Canada. From 2014 to 2016, he was a Scientist with the Telecommunication Circuits Laboratory, École Polytechnique Fédérale de Lausanne (EPFL), Lausanne, Switzerland. In November

2016, he returned to The University of Auckland to take up an academic post with the Department of Electrical, Computer, and Software Engineering, where he is currently a Senior Lecturer. His research interests include antennas, radiowave propagation, computational electromagnetics, and radar.

Dr. Austin was the recipient of the New Zealand Tertiary Education Commission Bright Futures Top Achiever Doctoral Scholarship from 2007 to 2011 and the Ministry of Business, Innovation and Employment Catalyst Strategic research grant from the New Zealand Government to investigate synthetic aperture radar on small satellites in 2019.



John E. Cater received the B.E. (Hons.) degree in mechanical engineering from the University of Auckland, Auckland, New Zealand, in 1997, and the Ph.D. degree from Monash University, Melbourne, VIC, Australia, in 2003 in the field of fluid mechanics.

He then moved to Europe to work on EU-supported aerospace research programs ENABLE, JEAN and COJEN creating future aircraft technologies and investigating aircraft noise reduction. He spent six years in Ireland and the U.K., working as a Research Fellow with Trinity College Dublin, Dublin, Ireland, and

Trinity College Cambridge, Cambridge, U.K., before becoming a permanent academic with Queen Mary, University of London, London, U.K. In 2008, he returned to The University of Auckland and joined Department of Engineering Science where he is currently an Associate Professor, leading work in computational mechanics and signal processing. In 2016, he became Deputy Head of Department. He has authored or coauthored more than 120 research articles in peer-reviewed journals and international conference proceedings, as well as three book chapters and two patents. He was one of the founders of the Auckland Programme for Space Systems, which gives undergraduate students the opportunity to design, build and launch nanosatellites to orbit. He was the Engineering Lead for New Zealand's first domestically constructed science satellite mission, launched from the Mahia peninsula in October 2020. His current research interests include electric propulsion for small satellites and modeling of thermal protection systems for reentry craft.



Gerhard Krieger (Fellow, IEEE) received the Dipl.-Ing. (M.S.) and Dr.-Ing. (Ph.D.) (Hons.) degrees in electrical and communication engineering from the Technical University of Munich, Munich, Germany, in 1992 and 1999, respectively.

From 1992 to 1999, he was with the Ludwig Maximilians University, Munich, Germany, where he conducted multidisciplinary research on neuronal modeling and nonlinear information processing in biological and technical vision systems. Since 1999, he has been with the Microwaves and Radar Institute,

German Aerospace Center (DLR), Wessling, Germany, where he started as a Research Associate developing signal processing algorithms for a novel forward-looking radar system employing digital beamforming on receive. From 2001 to 2007, he led the New SAR Missions Group, which pioneered the development of advanced bistatic and multistatic radar systems, such as TanDEM-X, as well as innovative multichannel SAR techniques and algorithms for high-resolution wide-swath SAR imaging. Since 2008, he has been the Head of the Radar Concepts Department, which hosts about 40 scientists focusing on new SAR techniques, missions and applications. He has, moreover, been a Mission Engineer for TanDEM-X and he made also major contributions to the development of the Tandem-L mission concept, where he led the Phase-0 and Phase-A studies. Since 2019, he is, moreover, a Professor with the Friedrich-Alexander-University Erlangen, Erlangen, Germany. He is the author or coauthor of more than 100 peer-reviewed journal papers, nine invited book chapters, more than 400 conference papers, and more than 20 patents.

Prof. Krieger has been an Associate Editor for the IEEE TRANSACTIONS ON GEOSCIENCE AND REMOTE SENSING, since 2012. In 2014, he was the Technical Program Chair for the European Conference on Synthetic Aperture Radar and as a Guest Editor for the IEEE JOURNAL OF SELECTED TOPICS IN APPLIED EARTH OBSERVATIONS AND REMOTE SENSING. He was the recipient of several national and international awards, including two best paper awards at the European Conference on Synthetic Aperture Radar, two transactions prize paper awards of the IEEE Geoscience and Remote Sensing Society, and the W.R.G. Baker Prize Paper Award from the IEEE Board of Directors.